



Analysis of the Internal Structure of Brenna Sandstone Samples with Respect to the Differences in Measured Quasi-elastic Moduli

Ivan Janeček¹ · Deepak Amban Mishra^{1,2} · Chitralkha Satheesan Vishnu^{1,3} · Kamil Souček¹ · Petr Hlaváček¹ · Dagmar Klichová¹ · Petr Martinec¹

Received: 27 October 2023 / Accepted: 19 February 2024
© The Author(s) 2024

Abstract

The Young's modulus and Poisson's ratio determined for the rocks under uniaxial or triaxial loading conditions represent necessary input parameters for solving many geotechnical tasks. However, these effective stiffness moduli, particularly the Poisson's ratios, measured on different samples sometimes substantially differ, even for visually compact and macroscopically homogeneous rock. This has been observed for Brenna sandstone, especially under conditions of conventional triaxial extensions. The aim of this study was, thus, to reveal differences in rock structure that could cause such behavior. Several complementary methods were used to investigate the structure of this sandstone: X-ray computed tomography (CT), visual analysis using optical scanning and stereo-microscopy, and a new method combining water jet erosion with these visualization techniques. Analyses of this structure revealed mechanically more resistant compact thick and adjacent thin weak layers. In rock samples, these layers have different patterns and orientations. To demonstrate the influence of layer orientation on effective stiffness moduli measured under different loading conditions, FEM calculations were performed for idealized structural models. The outcomes of this numerical analysis are in qualitative agreement with the results of the loading experiments and the layered structure revealed in the samples. The ability of the proposed method using water erosion to analyze the rock structure in detail was verified. The method offers an interesting alternative to standard visual and X-ray CT techniques. The numerical calculations indicate the importance of latent layered defects in sedimentary rocks for fine measurements of stiffness moduli (especially the Poisson's ratios) used as inputs for geotechnical applications.

Highlights

- Rock structure related to stratification has been analyzed by complementary methods.
- X-ray computed tomography revealed the irregular layered structure of the sandstone.
- A new method using water jet erosion of the rock surface confirmed the layers.
- Higher X-ray absorbance approximately corresponds to a higher mechanical resistance.
- A numerical model of the layers explains the differences in mechanical parameters.

Keywords Rock structure · Rock mechanics · Triaxial-stress state · Stratification · Sedimentary rocks · Sandstone · Water jet · X-ray CT

✉ Ivan Janeček
janecek@ugn.cas.cz

¹ Institute of Geonics of the Czech Academy of Sciences, Studentská 1768, Ostrava 708 00, Czech Republic

² Present Address: Department of Petroleum Engineering and Earth Sciences, Indian Institute of Petroleum and Energy, AUCE Road, Visakhapatnam, Andhra Pradesh 530003, India

³ Present Address: Borehole Geophysics Research Laboratory, Ministry of Earth Sciences, Karad, Maharashtra 415105, India

1 Introduction

Sedimentary rock materials can be found in many buildings and public structures. Therefore, knowledge of the structure of these widespread materials and their mechanical parameters is of considerable importance in civil or geotechnical engineering projects. In the case of the application of sedimentary rocks in underground construction (tunnels, or geothermal systems, etc.), it is necessary to take into account the fact that these rocks are exposed to a triaxial stress state. Therefore, in rock mechanics laboratories, mechanical parameters (such as Young's moduli and Poisson's ratios) of selected rock samples are also measured under different triaxial loading modes. However, the internal structure of seemingly compact samples can affect the resulting values of measured mechanical parameters. It is, therefore, desirable to study the internal structure of rock materials using various techniques and to estimate how its irregularities may manifest in the measured deformation response.

Sedimentary rocks often have a layered structure, at a high or low scale. In rock samples of decimeter-size (used for mechanical testing), thin layers (called *laminae*) having different material properties (grain size, mineral composition, density, content of clay) than adjacent basic rock material can often be found. The layers can sometimes be visually identified (on the surface of a rock sample) through a difference in color or shade. In other cases, they may be rather latent but still consist of material with different properties. Such layer structures can be found even in seemingly homogeneous sandstones (Hamblin 1965). In addition, a very thin weakened layer may be present at the interface of different materials. Such weak layers deform more under loading and may even develop into a crack (Lai et al. 2021). These layered inhomogeneities may affect the deformation in the rock, and thus influence the measured effective mean strains. The origin of these structures in different sedimentary rocks is variable and can be classified in many ways: primary (during diagenesis) and secondary (after lithification), or physical, chemical, and even biological origin, etc. Primary processes include recurring changes during the physical deposition of loose material or variable conditions of gradual chemical lithification. The secondary processes take place after the lithification. They include, e.g., physical and chemical weathering (mineral alterations, generation of cracks), the physical deposition of new external material in pores and cracks, crystallization from aqueous solutions, or even the activity of biologic organisms.

The anisotropy of physical properties (usually close to transverse isotropy), which can be observed in these rocks, is attributed to the internal layered arrangements of the grains and openings (coalescing pores or cracks) that are typically oriented along the bedding plane. For example,

the anisotropy of mechanical and acoustic properties has been investigated in Gatelier et al. (2002), Hu et al. (2017), Jamshidi et al. (2021), Song et al. (2017), Louis et al. (2003) and Wei et al. (2021). However, anisotropy of the rock may not be indicated by its visual inspection. Louis et al. (2003) commented that the sandstone which seemed to be the most homogeneous at macroscopic scale presented the intense anisotropy of P-wave modulus. In particular, the presence of cracks or weakened layers is of considerable importance for the strength and deformation of rocks. The role of weak layers at a macroscopic scale is known and has been studied. For example, the mechanical stability of slopes is affected by the orientation and thickness of such layers (Crusoe et al. 2016). Simulated weak layers affect the calculated ultimate bearing capacity of soils or rocks (Ziccarelli and Rosone 2021). Microscale weak layers can play a similarly important role in deformation and mechanical anisotropy of rock samples during mechanical tests (Louis et al. 2007, 2009; Baud et al. 2005). The structure of the Rothbach sandstone was investigated before and after a drained standard triaxial test using high-resolution CT (Louis et al. 2007, 2009). Rock samples were drilled in several orientations relative to the bedding plane. The influence of this orientation on strength and failure mode was determined, but the effect on stiffness moduli was not analyzed. Contact between the zones forming layers of different properties played an important role in rock failure. For example, in the CT scan of the sample with the oblique (45 degree) orientation of the plane, a shear band was observed that propagated from the sample surface close to an interface between two zones of contrasting porosities and average grain sizes (Louis et al. 2009).

Visual examination of the rock sample often does not reveal hidden small inhomogeneities or internal defects. The sample may appear to be relatively compact, and even the measured values of bulk density or ultrasound velocity may not show an anomaly that would indicate the presence of a defect or an inhomogeneous structure. However, knowledge of this structure and the defects in the material is decisive for the clarification of the mechanical behavior during measurements. Therefore, it is important to use and develop techniques that can well visualize such structures in rock materials.

In recent studies, researchers have frequently examined the deformation characteristics of rocks under various triaxial loading conditions, with a predominant focus on material failure. Surprisingly, only scant attention has been paid in the literature to comparing the behavior of effective stiffness moduli, notably Poisson's ratio. For example, stiffness moduli for several different loading paths are presented in the work (Panaghi et al. 2021). A procedure for the determination of stiffness moduli in the individual multiaxial modes, however, was not described. Hence, our

recent research (Janeček et al. 2024) was focused on the behavior of the measured effective tangential moduli of Brenna sandstone (macroscopically homogeneous) along several specific loading paths: Conventional Triaxial Compression (CTC), Conventional Triaxial Extension (CTE), Reduced Triaxial Compression (RTC), and Reduced Triaxial Extension (RTE) (Kwaśniewski 2012). Several additional repeated measurements on rock samples under the same load conditions were performed to test the variability of the determined effective stiffness moduli. The results of these experiments demonstrated a degree of variability in the quasi-elastic moduli. However, higher differences were observed for some tested samples. In particular, the effective tangential Poisson's ratios measured in CTE loading regimes showed significant deviations. (An example of such behavior is shown in Sect. 2.2). A plausible hypothesis is that this observation should be related to specific differences in internal rock structure. Thus, the natural motivation for further research was to confirm this hypothesis and reveal the essence of this structural variability. In the present study, we analyzed the structure of selected samples that showed the most pronounced differences in the determined quasi-elastic moduli. Various complementary methods were used for a detailed analysis of the layered structure of the Brenna sandstone. In addition to optical scanning of the sample surface, X-ray CT was applied. This non-destructive method is currently widely used for the laboratory study of rock materials. For example, this method has been applied to sandstone samples in the above-discussed works (Louis et al. 2007, 2009) and has recently also been used for the analysis of the structures of some other sandstones (Lindquist et al. 2000; Arns et al. 2001; Liu and Huang 2021). These recent experiments investigate sandstone even at stress or temperature conditions. X-ray CT scanning was, therefore, chosen as one of the well-established techniques for structural analysis of the Brenna sandstone in the new study.

Sometimes, however, even an X-ray CT scan does not have sufficient contrast to reveal hidden inhomogeneities in the sample or does not allow estimation of their mechanical properties. It is, thus, desirable to test other alternative techniques for visualizing rock structures with different material properties. Therefore, a CT visualization of the structure of Brenna sandstone was supplemented by a new method combining water jet erosion and optical scanning. The ability of a water jet to release material with lower strength is known, for example, from the removal of degraded concrete structures (Momber 2006; Hlaváček et al. 2019). A similar method was also used experimentally in the selective removal of bone cement during arthroplasty revisions (Honl et al. 2003; Nag et al. 2020). Yiyu et al. (2015) applied a disintegrating erosive water jet to sandstone and examined the

resulting failure pattern. Based on these experiences, the erosion of sandstone by a water jet of suitable parameters appeared to be a suitable candidate for displaying the structure of this rock.

In contrast to X-ray CT scanning, which is a fully non-destructive method capable of mapping the rock structure within the entire sample volume, the water jet erosion method has certain limitations. This technique can only analyze the structure within a narrow layer near the surface of the rock sample. Consequently, to obtain a structural map of the entire sample volume, it is necessary to disintegrate it through gradual cutting and continuous erosion. However, analysis of the erosion relief on the surface of the sample is usually sufficient to determine the typical thickness of the layers and trends in their orientations. This limitation is, therefore, not a major obstacle to the use of the method for analyzing the macroscopic structure of layers in rocks. Moreover, the water jet erosion method is not so time-consuming (an hour or two for sample geometry used in mechanical experiments) compared to a detailed X-ray CT scan (half of a day at least). Thus, this is a time- and economically less demanding method of textural analysis of test samples compared to widely used X-ray CT scanning. The water jet erosion method is also useful if the technique of visual analysis of the surface of the rock sample is not able to distinguish well the shade or color of the layers in the material, which all have different mechanical resistances. The practical application of the water jet erosion method to sandstones and other materials is discussed in Sect. 3.3.

In the present study of the Brenna sandstone, the results of all the visualizing methods discussed above were compared. The results of the analyzed microstructural composition and the visualized structure of the samples are discussed with respect to the differences in the mechanical parameters. Finally, a simple FEM analysis of the influence of idealized microstructural defects in the form of thin layers has been carried out to show the importance of their orientation on measurements of mechanical parameters.

2 Experimental Technique and Methods

2.1 Description of the Investigated Rock

In this experimental work, the sedimentary rock, Brenna sandstone (Beskid of Silesian region, Poland, Kwaśniewski and Takahashi 2010), was analyzed. This type of glauconitic sandstone occurs in the Middle Member of the Godula Formation of the Outer Western Carpathians flysch (Vavro et al. 2016). The framework of the Brenna sandstone consists mainly of stable components: quartz

(49%), quartzite (18%), chert (4%), and other rock fragments (8%). The non-stable component includes: micas (3%), feldspar (2%), and unstable rock fragments (4%). The rock matrix contains: phyllosilicates (5%), quartz (4%), carbonate (2%), and glauconite (1%). The density of the solid phase measured by He-densitometry falls in the interval from 2630 to 2650 kg/m³. The porosity of this sedimentary rock is about 7% ($\pm 1\%$). Some details about the petrography of this sandstone can be found in Janeček et al. (2024). Thin laminae of deposited clay matter can be found in this otherwise very compact material. The formation of these inhomogeneities is accompanied by diagenetic cementation of the pores and matrix, while weathering or biogenic mineralization do not play a role.

2.2 Experimental Determination of Mechanical Moduli

Mechanical parameters (Young's moduli and Poisson's ratios) of cylindrical rock samples (diameter/height = 50 mm/100 mm) were previously determined using two types of triaxial tests, CTC and CTE starting at the given confining pressure p_0 . In CTC tests, the axial stress σ_{ax} was increased by constant stress rate $\dot{\sigma} = 0.25$ MPa/s that corresponds to ISRM suggestions. The same constant rate $\dot{\sigma}$ was used for increasing the lateral stress σ_{lat} in the CTE tests.

For the implementation of these loading conditions, an experimental device for triaxial tests designed by the company MTS Corporation was used. This device consists of a triaxial chamber (maximum pressure: 140 MPa) and a load frame (limit forces: 4.6 MN/2.3 MN at compression/tension; frame stiffness: 1050 MN/m) with a hydraulic piston. A load cell inside the chamber was used to measure the axial stress (limit force: 2.6 MN). A more detailed summary description of this experimental device, including its schemes and photos, can be found in the appendix of the work (Janeček et al. 2024). During the testing, the axial strain (ϵ_{ax}) and lateral strain (ϵ_{lat}) of the sample were measured through a dual axial extensometer and a circumferential chain extensometer. Figure. 1 shows a rock sample with the installed extensometers before measurement in the triaxial cell.

The effective stiffness parameters of rock samples were determined under the assumptions of the commonly used basic approximation of idealized quasi-elastic, homogeneous, and isotropic material. Under these assumptions, the effective Young's modulus and Poisson's ratio can be calculated through formulas: $E = d\sigma_L/d\epsilon_L$ and $\nu = -d\epsilon_T/d\epsilon_L$, where ϵ_L and ϵ_T are longitudinal and transversal strains with respect to the direction of applied stress (i.e., the stress with magnitude σ_L is acting along a selected axis L). For CTC tests, the following simple identities are

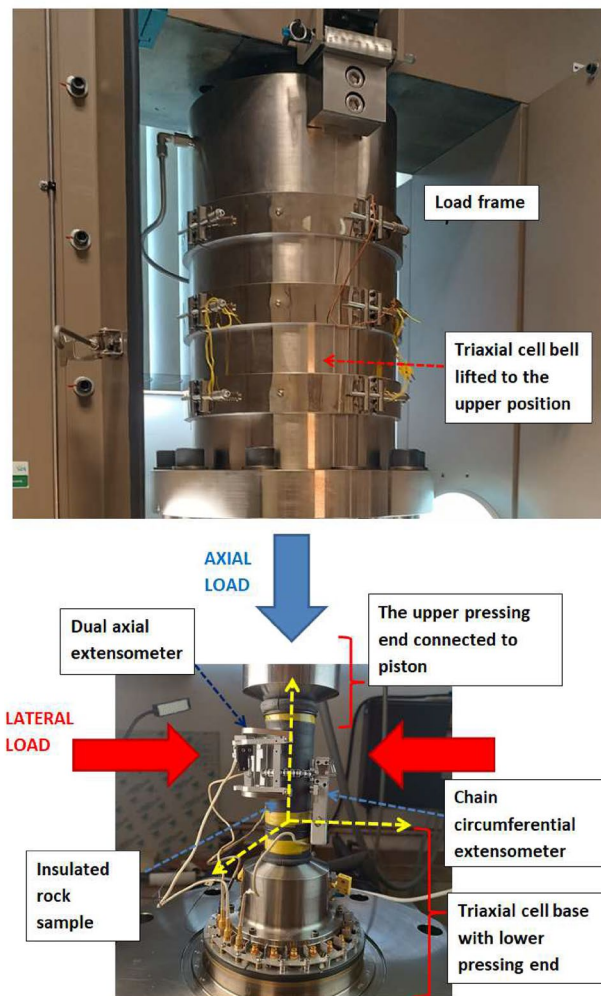


Fig. 1 Important parts of the experimental equipment and the installed rock sample (yellow arrows—reference coordinate system) (Colors online)

valid: $d\epsilon_L = d\epsilon_{ax}$, $d\epsilon_T = d\epsilon_{lat}$, and $d\sigma_L = d\sigma_{ax}$. For CTE tests, the formulas based on decomposition of strains can be applied: $d\epsilon_L = d\epsilon_{lat} - d\epsilon_{ax}/2$, $d\epsilon_T = d\epsilon_{ax}/2$, and $d\sigma_L = d\sigma_{lat}$ (Janeček et al. 2024).

Some of the Brenna sandstone samples showed visible differences in mechanical behavior, although they were deformed by the same stress mode of loading. In Fig. 2, this situation is demonstrated by the variability of stress–strain curves of selected rock samples.

The Table 1 shows the corresponding moduli determined by the procedure described above.

2.3 Visualization of Layers in Rock Samples

For an in-depth analysis focused on the presence of potential defects, layers, or irregularities in the rock structure, two cylindrical samples were selected that showed significant

Fig. 2 Experimental stress–strain curves covering the quasi-elastic region. The axial and lateral strains in the graphs correspond to two types of additional loading, which were applied to the sandstone samples after their initial isotropic compression to a pressure of 60 MPa: **a** axial loading (CTC stress path) and **b** lateral loading (CTE stress path). In the upper graph (a), the range of lateral strains presented in the lower graph (b) is inserted for comparison. Note to the curves of the dependence $\sigma_D(\epsilon_{ax})$ in the graph a The curve part of the initial compaction of sample 1/I under the CTC loading regime was apparent compared to those of samples 3/IIIa and 5/IIIb. However, the linear slopes of the curves of all three samples at about 60 MPa were very close (Colors online)

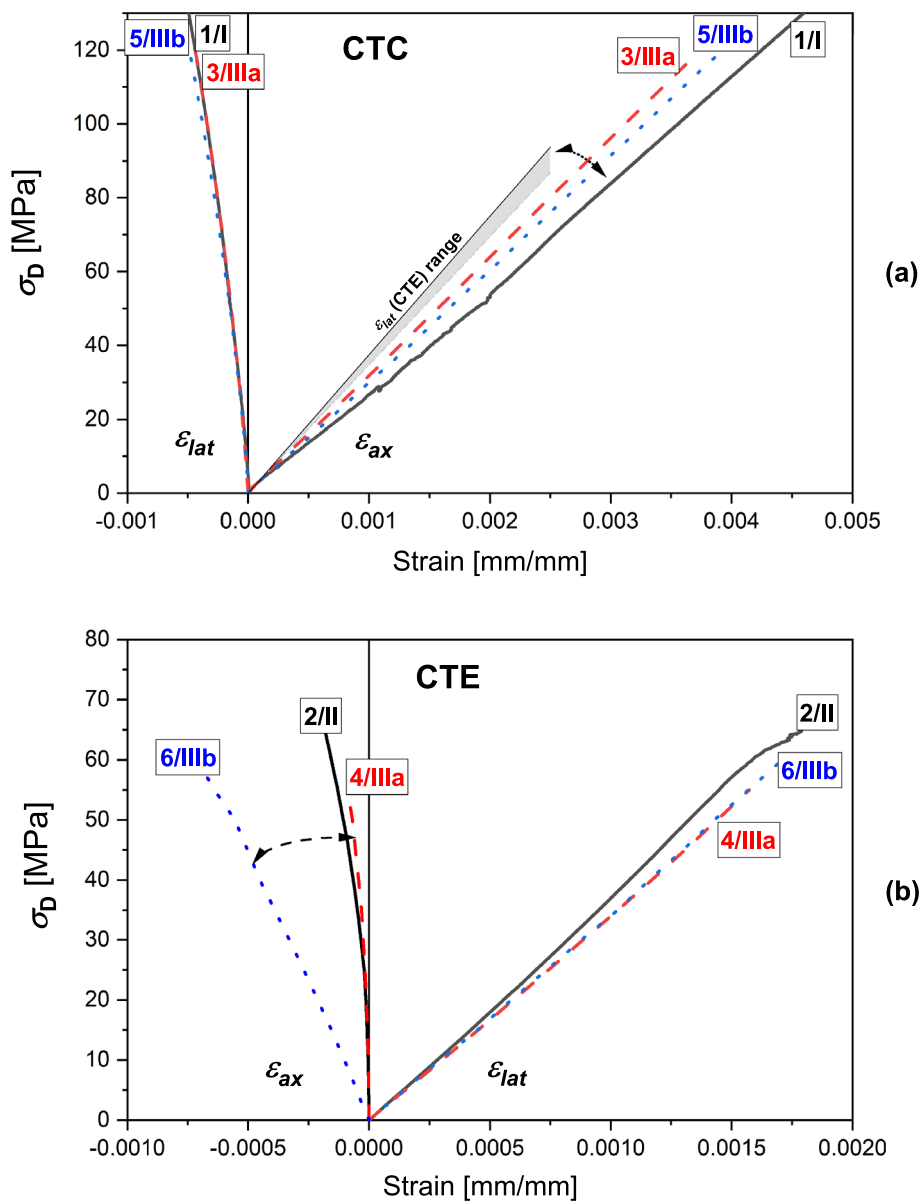


Table 1 Several representative effective stiffness moduli from conventional triaxial paths: E_{load} —loading Young’s modulus (the mean value of the modulus in the stress region of the approximate linear

dependence of strain ϵ_L on loading stress σ_L); ν_{load} —loading Poisson’s ratio (the value range of the monotonic increase of the modulus in the same stress region)

Sample	Test	E_{load} (GPa)	ν_{load} range	Sample	Test	E_{load} (GPa)	ν_{load} range
1/I	CTC-60 MPa	30.5 ± 0.3	0.11–0.12	2/II	CTE-60 MPa	36.4 ± 0.6	0.02–0.06
3/IIIa	CTC-60 MPa	32.2 ± 0.3	0.11–0.13	4/IIIa	CTE-60 MPa	33.6 ± 0.3	0.02–0.04
5/IIIb	CTC-60 MPa	30.9 ± 0.5	0.12–0.14	6/IIIb	CTE-60 MPa	28.7 ± 0.5^a	0.17–0.18

^aThe lower value of the effective CTE Young’s modulus for sample 6/IIIb compared to the values for samples 2/II and 4/IIIa is affected by the high value of the determined effective Poisson’s ratio

differences in their deformation during identical mechanical CTE tests (initial isotropic pressure $p_0 = 60$ MPa): sample 4/IIIa and sample 6/IIIb. For these samples, the Young's modulus showed less deviation compared to the Poisson's ratio, which is considerably different. In these tests, the differential stress was limited to a maximum value of about 60 MPa. This limitation prevented the fragmentation of the samples by final failure.¹ For this reason, it was possible to carry out an additional detailed analysis of the internal structure of the rock in the samples used in these tests.

The internal structure of the selected sandstone samples was visualized by several scanning techniques. The rock samples were first investigated by X-ray computed tomography (CT). The "X TH 450" system from *Nikon Metrology* with a 450 kV X-ray source and a 2000 × 2000 Px flat panel was used to study the internal structure of the sandstone samples. The settings of the tomographic system were tuned to achieve the best possible contrast for the CT images.

In the next step, a more detailed analysis of the layered structure of both spatially close rock samples (4/IIIa and 6/IIIb) from the CTE experiments was done. The analysis focused on the investigation of representative cross-sections of both samples. Each such cross-section corresponds to a real cut of the cylindrical sample along a selected central axial plane. (i.e., the original cylinder was split into two semi-cylinders). For each sample, a pair of new surface areas was created by this cut. These surfaces were then examined by several analytic methods. One surface area of each pair was optically scanned to analyze differences in colors and their saturation and to evaluate the morphology of the visualized layers. Then a CT scan was performed closely below this surface area for comparison. Finally, selected parts of the analyzed material (with visually discernible differences in its structure and properties) were inspected by infrared spectroscopy, optical microscopy, and scanning electron microscopy with analysis of elements.

In addition, the relative local firmness of the rock material in the second surface area (originally adjacent to the first) was investigated through a new method based on a combination of the erosive effects of a water jet and the optical scanning of the surface relief generated by this erosion. The grains fixed in the material by weaker bonds were removed after the application of the water jet. The newly created surface relief was analyzed using an optical 3D scanner. Stereo-microscopy was used to visualize selected details in the relief.

The process of controlled erosion of the sandstone surface was carried out using a multipurpose water jet device equipped with a high-pressure pump *PTV 75-60* (PTV). A simplified scheme of this device with an illustrative photo is

given in Fig. 3. The movement of the jet on the sample surface was controlled by an X–Y cutting table *PTV WJ2020-2Z-1xPJ-2D* (PTV) with a tilting cutting head (developed for cutting with a high-speed water jet) and a computer control system. Appropriate parameters for the generation of the erosive water jet (especially water pressure) were tuned using initial experiments on test samples. The aim of these experiments was to achieve a pronounced relief (with a height difference of approx. 1 mm). The water jet used for the final surface analysis of samples was generated by a nozzle (diameter 0.33 mm) at a water pressure of 40 MPa and subsequently formed by a focusing tube with an inner diameter of 1.02 mm. The generated water jet was focused from a distance of 50 mm perpendicularly to the investigated surface of the sample. During the erosion of the surface, the jet moved at a speed of 2 m/min along the original axial direction of the sample. Forward and backward movements alternated with perpendicular shifts of 1 mm to cover the entire surface area of the sample. For the visualization of the generated surface relief, a *VHX 5000* digital microscope (Keyence), a *Go!Scan* portable 3D scanner, and *VXelements* software (Creaform) were used.

2.4 Numerical Model of the Deformational Behavior of a Sample with Idealized Layered Inhomogeneities

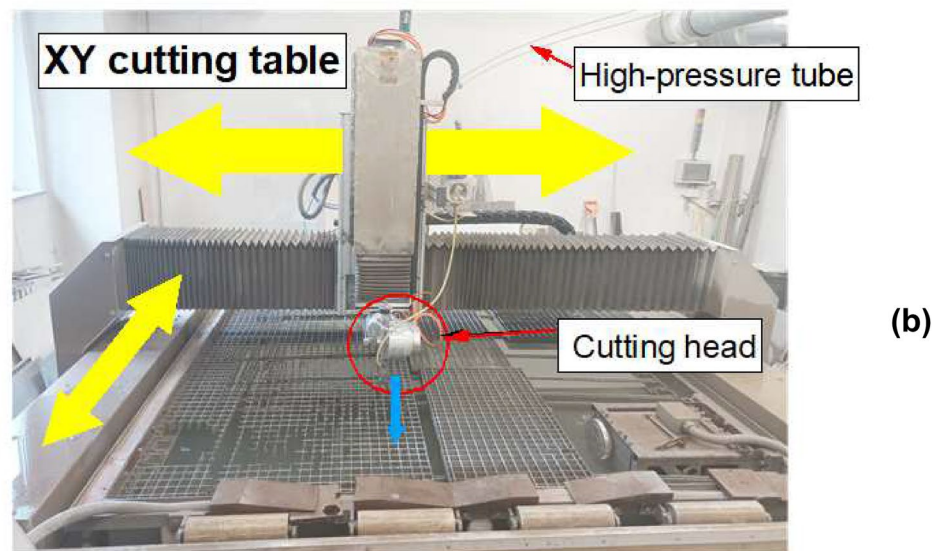
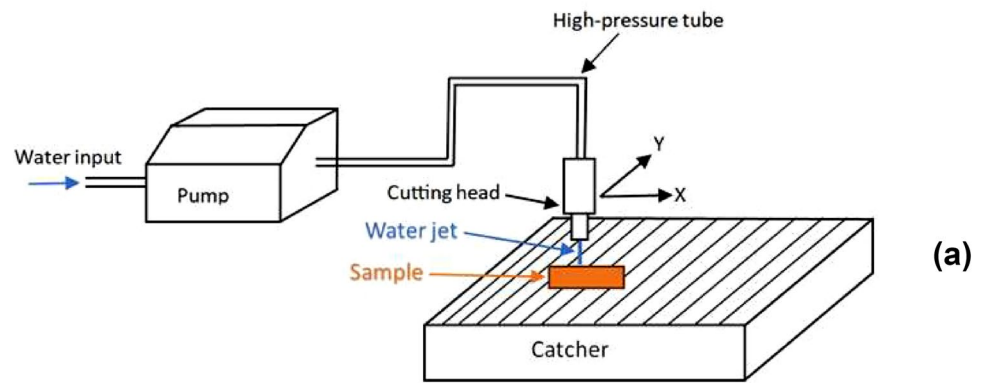
To demonstrate how the orientation of the layers in a material or some of their mechanical properties can in principle affect the values of the effective stiffness moduli (Young's modulus and Poisson's ratio) measured under a specific load, idealized numerical models were prepared. For simplicity of calculations, 2D FEM models of the sample in the shape of a rectangle (10 cm × 5 cm) were used to analyze the role of the local inhomogeneities in the form of layers in the sample in its deformational behavior. The numerical calculations in this study were performed using FEM software (*Agros2D*) developed for the numerical solution of physical fields based on the *HERMES* library (Karban et al. 2013). In addition, a standard linear (quasi-elastic) isotropic material model was considered for all parts of an inhomogeneous sample. Each such part was described by a given pair of input parameters: the Young's modulus and the Poisson's ratio. Despite this local isotropy, a suitable composite-layered model material can even describe anisotropic behavior.

The quasi-elastic linear description is widely used in geotechnical practice as a basic approximation for describing the deformation behavior of rock for stresses that are sufficiently low compared to the peak stress.² The proposed

¹ The typical uniaxial peak strength of this sandstone is about 120 MPa.

² It is commonly neglected that, unlike longitudinal deformations, transversal deformations typically show some more pronounced deviations from linearity.

Fig. 3 Water jet device: **a** Scheme of the equipment used for controlled erosion of a sandstone surface by a high-pressure water jet; **b** photo of the XY cutting table (made by PTV company) with installed cutting head (Colors online)



model focuses just on the quasi-elastic region of stress. Therefore, basic rock material, as well as material that has undergone greater silicification, are good candidates for such a description. Even in the case of a weakened material, its deformation under static conditions may not necessarily be modeled by the plasticity theory, damage model, or contact problem. The purpose of the proposed illustrative model is to investigate the trends in sample deformation, which are given by displacements of the sample's stiff parts connected by a narrow, weak interlayer. For considered purely loading conditions, this interlayer can roughly be modeled using the linear model with the Young's modulus being substantially lower compared to the rest of material. A significant advantage of such a rough linear description is the simplicity of calculations and the good convergence of the numerical solution in comparison with, for example, contact problems.

In this simplified linear model, the deformational responses to the initial isotropic and the additional axial or lateral stress can be superposed. Therefore, this additional loading can be simulated separately. The initial undeformed state of the model sample in this simulation,

thus, corresponds to the zero differential deformation in the state after the initial isotropic compression. Differential deformation during subsequent quasi-static differential loading in the CTC or CTE test is modeled through static axial or lateral compression. Therefore, for the applied linear FEM description, the effective moduli calculated from the deformation under this axial or lateral loading will be referred to as the model results for the CTC or CTE differential loading, respectively.

Numerical calculations were focused on situations where the inhomogeneity in the model sample consisting of a base material is composed of the strong thick layer (width 0.59 cm) and the adjacent weak narrow layer (width 0.01 cm) interrupted by narrow rectangular interconnections (mid, left and right border of the thin layer; horizontal width 0.001 cm; a model of grain joints) of the base material with the strong layer. The thickness of the thick layer roughly corresponds to the thickness of the silicified layers found in the samples of Brenna sandstone. The selected value of the weak layer thickness is a model compromise. This layer simulating a weakened contact must

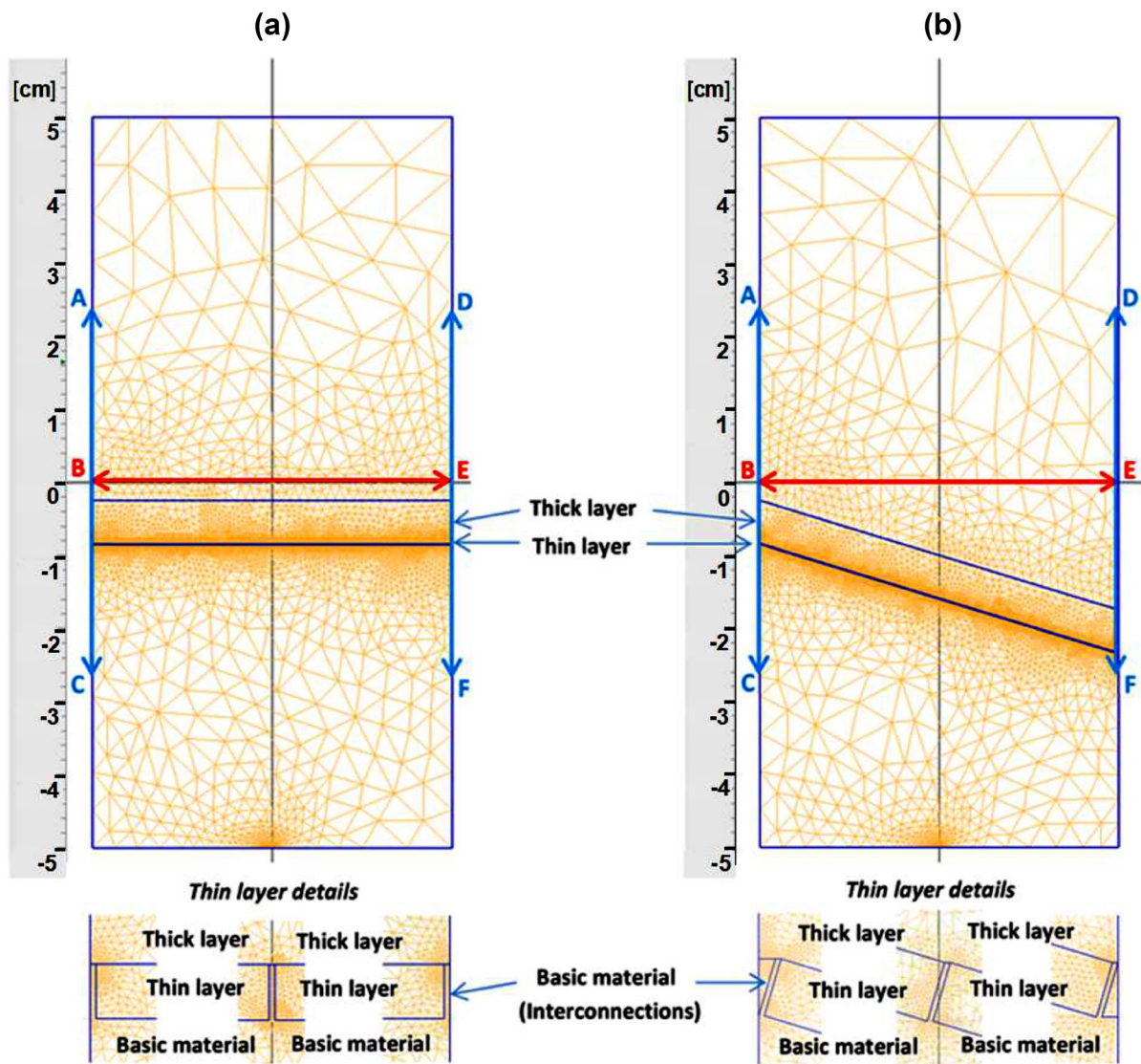


Fig. 4 Geometries of two model samples with layers and gauge lengths. Rectangular sample (5 cm \times 10 cm) with: **a** horizontal bi-layer, **b** oblique bi-layer (declination angle of about 17 degrees). Legend: AC—left axial gauge length (5 cm; AB = BC = 2.5 cm), DF—right axial gauge length (5 cm; DE=EF=2.5 cm), BE—lateral

gauge length (5 cm); “Thin layer details”—zoomed-in view of the geometry of the left, middle, and right interconnections. *Note:* The geometrical and material parameters of the layers, and basic material are described in the text (Sect. 2.4)

be substantially thinner than the strong layer. However, a layer thickness that is too small would require a local denser FEM mesh and would, thus, lead to higher computational requirements. The orientations of this bi-layer in the performed simulations were inspired by the different arrangements of the layer structure in the investigated real samples (discussed in Sect. 3). Two qualitatively different orientations of the bi-layer in the simulated sample were considered: horizontal and oblique with a declination angle of about 17°. The geometries of two idealized model samples with layers are shown in Fig. 4. The vertical position of the idealized bi-layers was -0.25 cm from the central horizontal section, i.e., close to the position of

the horizontal gauge length and within the range of both vertical gauge lengths to see the maximum effect on the simulated measurement, but slightly off-center to avoid a symmetric situation.

In the presented model calculations, the sample consists of the basic material with $E = 40$ GPa and $\nu = 0.10$. The chosen values of its mechanical parameters are not far from the effective values determined for the real sandstone tested in the experiment (Table 1). The resulting deformations of the homogeneous model sample containing only the basic material are, thus, comparable to those in the experiment. The investigated instances of inhomogeneous samples included thick and thin layers

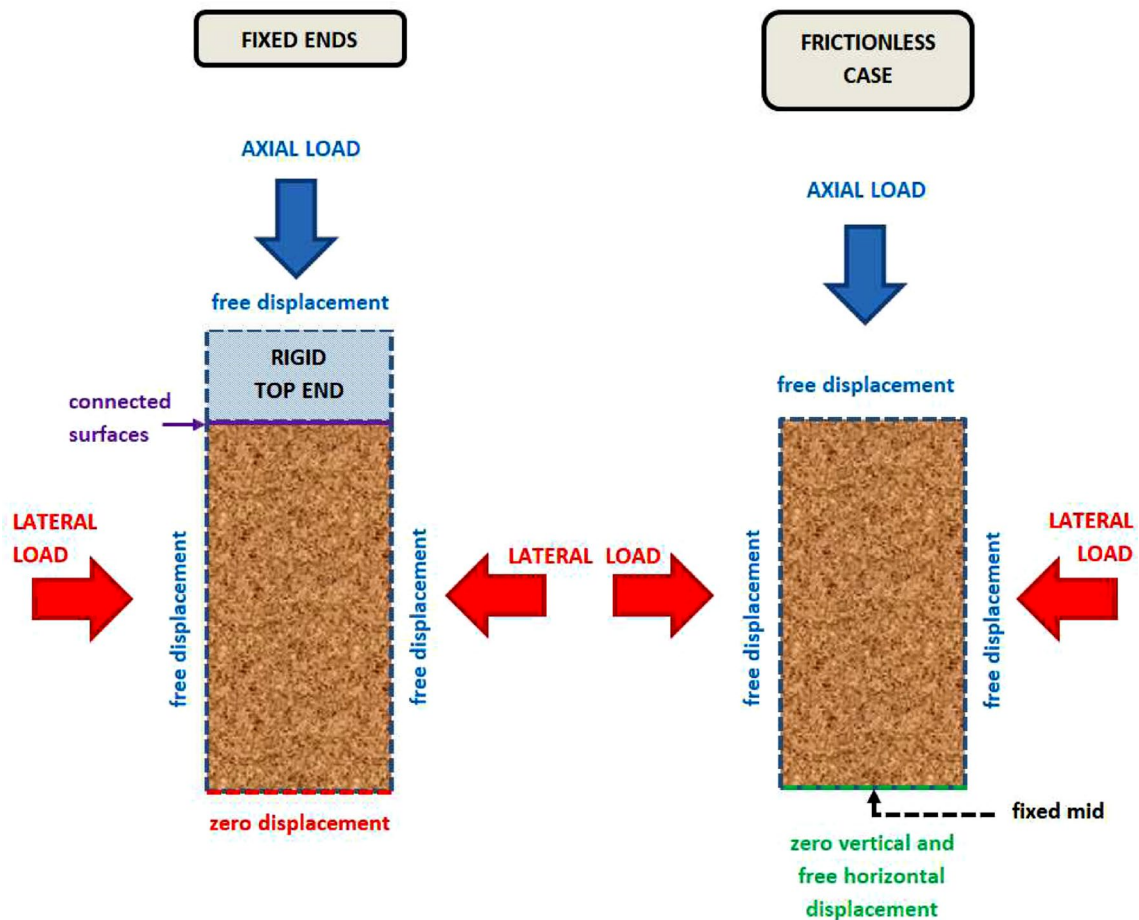


Fig. 5 Numerical conditions of the FEM model of the sample (Colors online)

with parameters different from the base material. Since the goal of the model is only a qualitative description of the mechanical behavior of the material, the values of these parameters are chosen ad hoc to simulate qualitatively different mechanical properties of the layers. Local differences in the magnitudes of mechanical bonds in a rock sample are simulated by setting the magnitude of the Young's modulus in these model layers. The Poisson's ratio of a material is influenced by its internal structure. However, a specific internal micro-structure of the layers is not considered in this illustrative qualitative model. Therefore, for simplicity, a very small nonzero value was defined for the Poisson's ratio of both layers. The thick layer consists of a stiffer material ($E_S = 50$ GPa, $\nu_S = 0.01$) modeling a dense matter with increased silicification. A higher degree of silicification leads to stronger mechanical bonds between the grains in the rock. Therefore, the Young's modulus E_S was chosen somewhat higher than that of the basic material. The thin layer of a weak material ($E_W = 1$ GPa, 0.5 GPa, and 0.1 GPa, $\nu_W = 0.01$) simulates a weak connection at the interface

between the thick layer and the basic material. This weak connection corresponds to a region of a latent fracture surface in the simulated rock sample. The material in this region can often be characterized by the presence of slit pores, which significantly contribute to its weakening. Therefore, the values of the modulus E_W were adjusted to be substantially lower compared to the Young's modulus of the basic material. The several different E_W values model the degree of the weakening of this connection. Continuity conditions are imposed on the displacements of all internal boundaries that correspond to the interfaces between two different materials in the sample.

Additional boundary conditions were defined for the numerical calculations to model the situation during the measurements (Fig. 5). Specific sets of conditions were imposed on the displacements to simulate the contact with pressing ends in the axial loading system and the contact with the confining fluid. Left and right rectangle borders simulating the sample surface, which is under the pressure of confining media, are always considered free (i.e., no condition for displacement, but defined stress at the boundaries).

For horizontal displacement at the top and bottom borders of the model sample, two different conditions were used to estimate the role of friction at the contact areas between the sample and the pressing end. The first condition simulates the situation without friction, while the second one models a sample fixed at the pressing ends. The first case involves free displacement at the top sample border, free horizontal displacement at the bottom sample border with the exception of its central part,³ and zero vertical displacements at the bottom border. In the second case, the model sample is fixed to the rigid top pressing end, which is modeled as a rectangle (2 cm × 5 cm) fixed by its bottom border to the top sample border. The conditions on displacements are: free top border of the rigid pressing end, and zero displacements of the bottom sample border. The applied axial stress σ_{ax} acts in the vertical direction on the upper boundary of the 2D sample or, in the second case, on the upper boundary of the rigid pressing end. The lateral stress σ_{lat} is applied perpendicular to the left and right boundaries of the 2D sample. The orientation of all applied stresses corresponds to the sample compression.

The calculated axial displacement was the average of the changes in the gauge lengths (5 cm) centered at the left and right sample borders; the lateral displacement was determined as a change in the width (5 cm) of the sample at its center. These gauge lengths are marked in Fig. 4. The displacements were determined at simulated static states under CTC loading ($\sigma_{lat} = 0$ MPa, $\sigma_{ax} = 50$ MPa) and under CTE loading ($\sigma_{lat} = 50$ MPa, $\sigma_{ax} = 0.5$ MPa⁴). The effective mean axial and lateral strains were obtained from the axial and lateral displacements after dividing them by the known initial gauge length values (5 cm).

For the introduced linear 2D model, corresponding effective Young's moduli and Poisson's ratios were calculated by their standard definitions: $E = \sigma_L / \epsilon_L$ and $\nu = -\epsilon_T / \epsilon_L$. For axial loading (CTC test): $\epsilon_L = \epsilon_{ax}$, $\epsilon_T = \epsilon_{lat}$, and $\sigma_L = \sigma_{ax}$. For lateral loading (CTE test): $\epsilon_L = \epsilon_{lat}$, $\epsilon_T = \epsilon_{ax}$, and $\sigma_L = \sigma_{lat}$.

3 Results and Discussion

3.1 Visualization of Brenna Sandstone Structure

First, 3D maps from X-ray CT scans of both investigated rock samples were analyzed. 2D maps of the three perpendicular sections of the 3D maps for both samples are shown in Fig. 6. These maps contain the dark regions corresponding

to higher absorption of the X-rays. To achieve better visualization of the morphology of these structures, contrast pseudo-colors were used in the pictures. These contrasting pictures reveal the layered character of these structures in both samples. The structures typically take the form of almost horizontal layers, but the CT scans of the sample 6/IIIb also show some local structures, which are rather of a vertical orientation. In the event that the inhomogeneities identified through the X-ray CT images correspond to layers having different mechanical parameters, the observed irregularities in their orientation could be responsible for the different deformation behavior of the two compared samples. Therefore, it was necessary to estimate the mechanical properties of the layers. For further analysis of the nature of these internal structures, the samples were cut into two semi-cylinders. The flat surfaces of these semi-cylinders were analyzed by the methods described in Sect. 2.3.

Visualizations of the layered structures in the samples using all the above-described methods (including photo scans and erosion by water jet) are compared in Fig. 7. The layered structure can be identified visually in suitable illumination at some places on the sample surface as irregular darker lines associated with thin layers, which are mostly oriented close to the horizontal direction. On the original photo scan in perpendicular illumination (using a visual scanner), (Fig. 7a), these layers are rather latent. However, some of them can be identified on a photo scan with increased contrast (Fig. 7b). On the other hand, the layered structure is very clearly visible in the X-ray CT scans (Fig. 7c), where the bright layers correspond to areas of higher X-ray absorption. The same areas can be well identified by their shape and location with the areas which had the least erosion of the rock material by the scanning water jet (Fig. 7d, e).

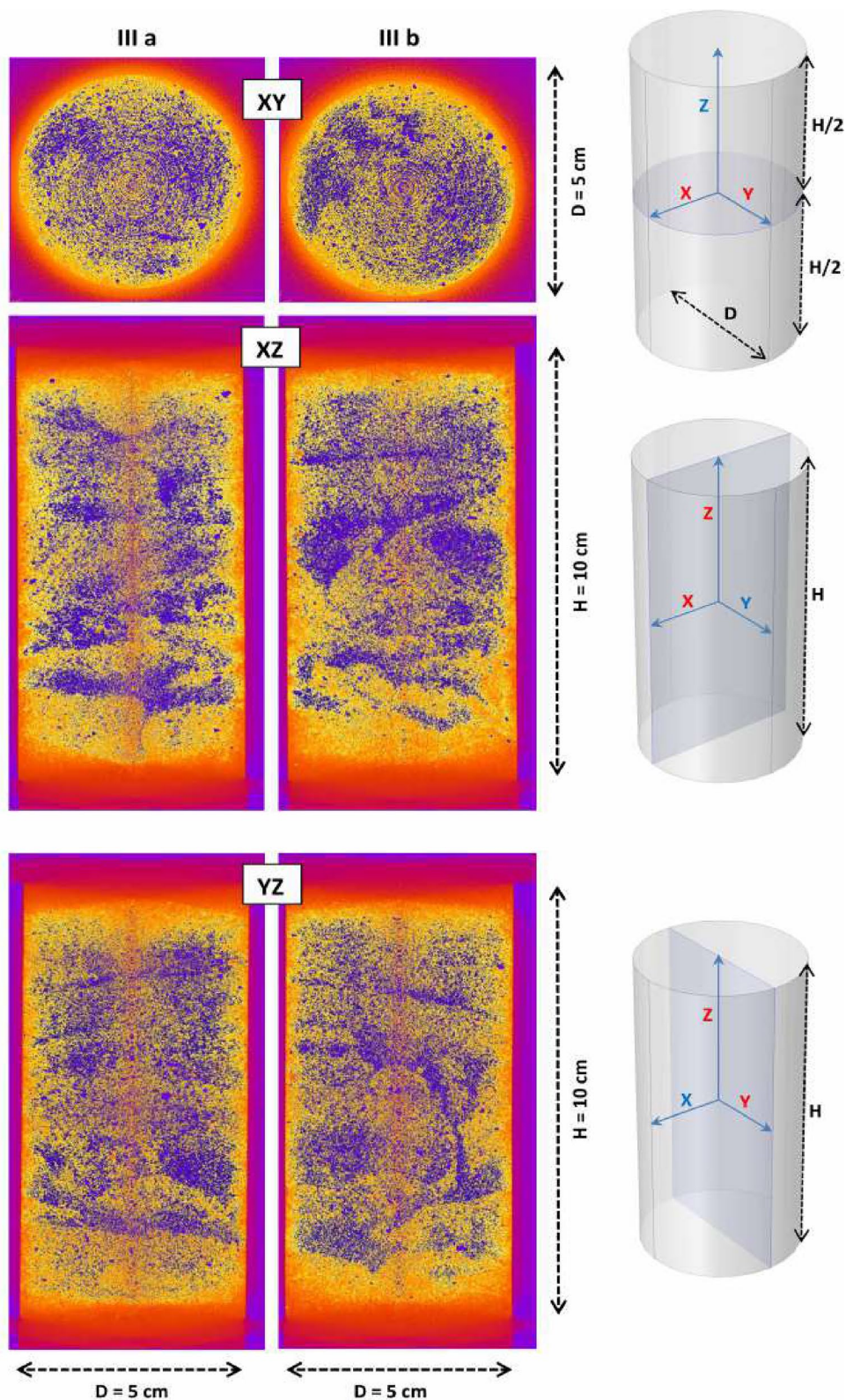
This structural coincidence can be explained by the fact that the areas containing the rock material of higher density have higher X-ray absorbability, and this dense material is also more compact and firmer, so its higher mechanical resistance and stiffness can also be expected. A detail of a layer structure in the analyzed sandstone is shown in Fig. 8. The shapes of the layers with different saturation and color in the visual scan of the non-eroded surface (Fig. 8a) and the X-ray scan of the adjacent section (Fig. 8c) correlate quite well. The same areas can be better compared using the contrasting artificially colored images: stereo-photo of the eroded surface (Fig. 8b) and X-ray CT scan (Fig. 8d). Differences in the local X-ray absorbability as well as in the mechanical resistance of observed layers are clearly visible in these images. These differences originate especially from a different level of solidification during the diagenesis of the sediment. On the contrary, the chemical composition of the compact stiff layers was not visibly different from the adjacent material.

On a microscopic scale (Fig. 9a), this compact material consists of grains (rather of the larger dimensions), which

³ This fixation is necessary for a definite numerical solution.

⁴ The value corresponds to the small initial load used in the real experiment and can be neglected under a big load applied during the measurement.

Fig. 6 X-ray CT analysis. Three sections of two cylindrical samples (4/IIIa and 6/IIIb loaded by identical CTE modes) of Brenna sandstone obtained by X-ray computed tomography (contrast pseudo-colors): transversal section XY through the center of the cylinder (top), and two perpendicular axial sections XZ (middle) and YZ (bottom). Dark areas on a bright background represent regions of higher X-ray absorption (Colors online)



are strongly bound through intense crystal inter-growth and by cement material with the almost continuous matrix. The material (mostly consisting of small grains) with weaker

inter-grain bonds was more affected by water jet erosion (Fig. 9b). In regions with this less-resistant material, the development of natural fracture surfaces is more probable.

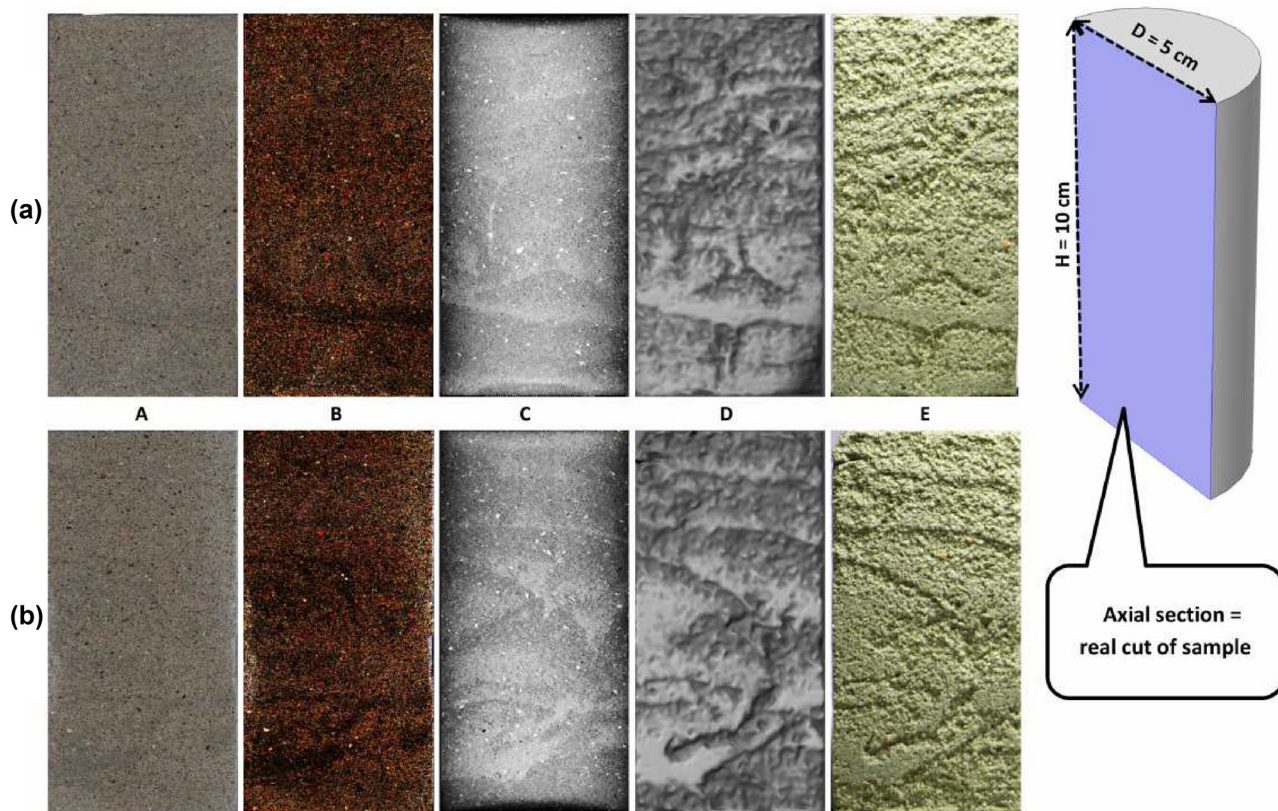


Fig. 7 Visualization of layers in sandstone samples. Comparison of several visualizations of real axial cuts for the samples in experiments a) 4/IIIa (top set of pictures) and b) 6/IIIb (bottom set of pictures): **A** Photo scan—a visual scan of one surface area created by a cut of the sample; **B** contrast scan—the original photo scan with improved saturation and increased contrast to highlight the layers observed visually; **C** X-ray CT scan just below this surface area (lighter areas correspond to higher absorption in regions with denser material); **D**

WJ-Relief map—a map of the depths in the relief, which was created after the erosion of the originally adjacent flat surface of the opposite half-cylinder by a water jet (the brightest areas represent the highest positions, which correspond to the regions containing the rock material that is the most resistant to this erosion); **E** relief photo—photographs of the same relief in the top illumination to highlight the observed layered structure. *Note:* The pictures **D**, **E** of the opposite surface area are mirrored for better comparison (Colors online)

The highest probability of this process could be expected at well-pronounced borders of the stiff and weak material. In the micrograph of a thin section (Fig. 9c), the slit-like pores at the boundary between the two layers are clearly visible. An example of a realized natural fracture surface in the studied sandstone is shown in the SEM micrograph in Fig. 9d.

From a comparison of the distribution of the less-resistant material and the orientations of the layers in both samples, it can be deduced that their distinct mechanical behavior results from the observed differences in the local structure of the rock. Identification of detailed microscopic processes leading to different deformations of both samples is not easy. However, the probable scenario can be described as follows.

The sample 4/IIIa shows less pronounced irregularities (especially an inhomogeneity of the horizontal direction in its bottom half) than the sample in experiment 6/IIIb (layers with a greater slope). The dominant horizontal orientation of the layers in sample 4/IIIa may explain the smaller transversal deformation (i.e., in the axial

direction in the CTE mode) during lateral compression as the indirect axial compression of weak layers plays the main role. On the other hand, the orientations of the layers in sample 6/IIIb typically demonstrate a large deviation from the horizontal direction. Therefore, in the 6/IIIb case, a higher transversal deformation can be observed as a consequence of the shearing processes.

This plausible scenario calls for a more exact theoretical analysis of the measured deformational response of samples containing particular types of inhomogeneity. However, the preparation of an accurate numerical model based only on the determined geometry of the layers without detailed knowledge of the exact local mechanical parameters and internal bonds is a hardly solvable task. Therefore, an analysis of the role of selected representative layer orientations in the mechanical behavior of rock samples was performed using a simplified numerical model of inhomogeneous samples described in Sect. 2.4).

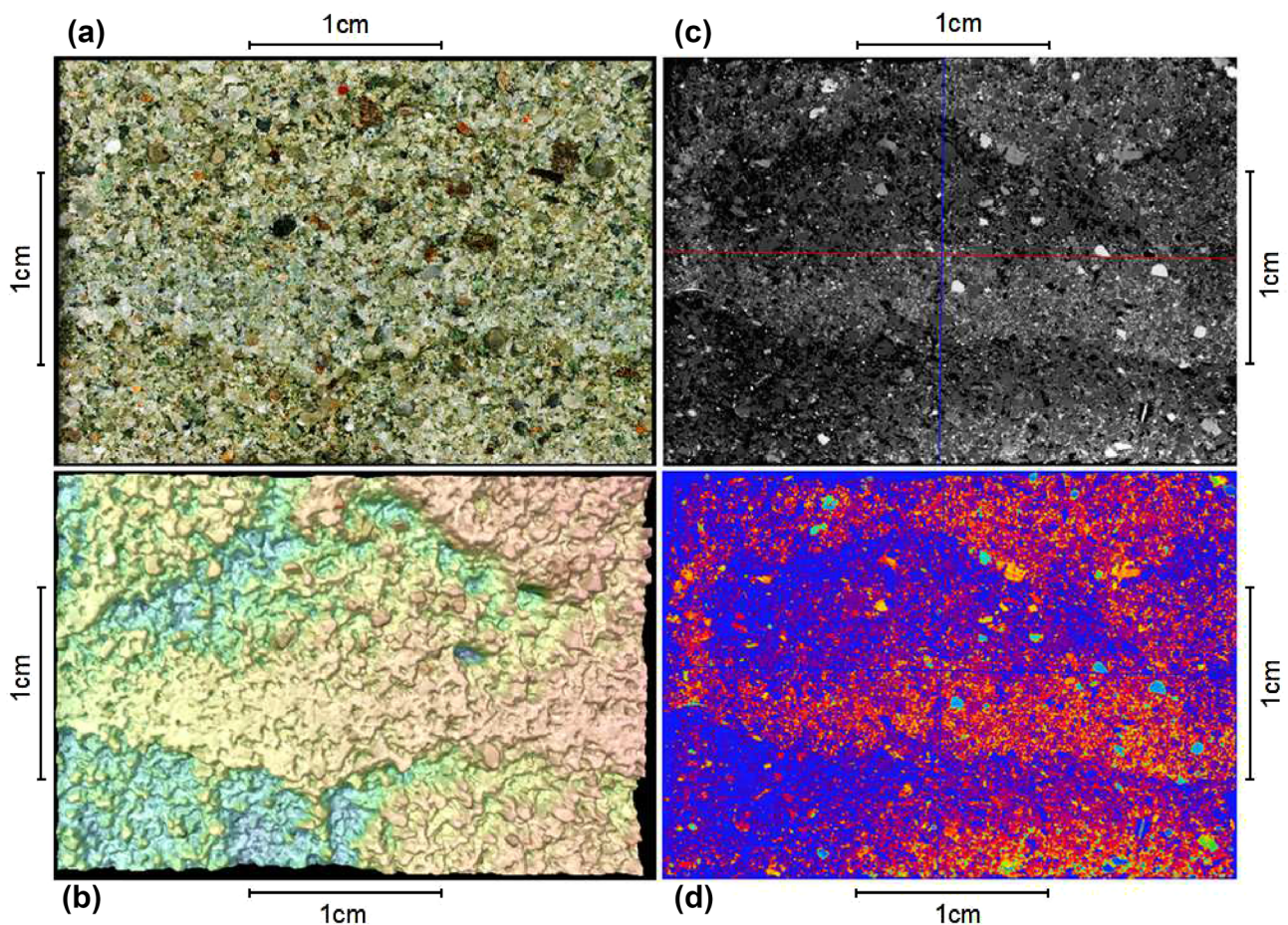


Fig. 8 Detail of structure of the pronounced layer at the bottom part of sample 4/IIIa: **a** Photo-micrograph of the eroded surface obtained using a stereo-microscope—(enhanced contrast; mirrored); **b** the same snap-shot with a semitransparent color map of depths—(blue color corresponds to a lower vertical position of the surface; mirrored); **c** contrast X-ray CT scan of an adjacent vertical thin slice that

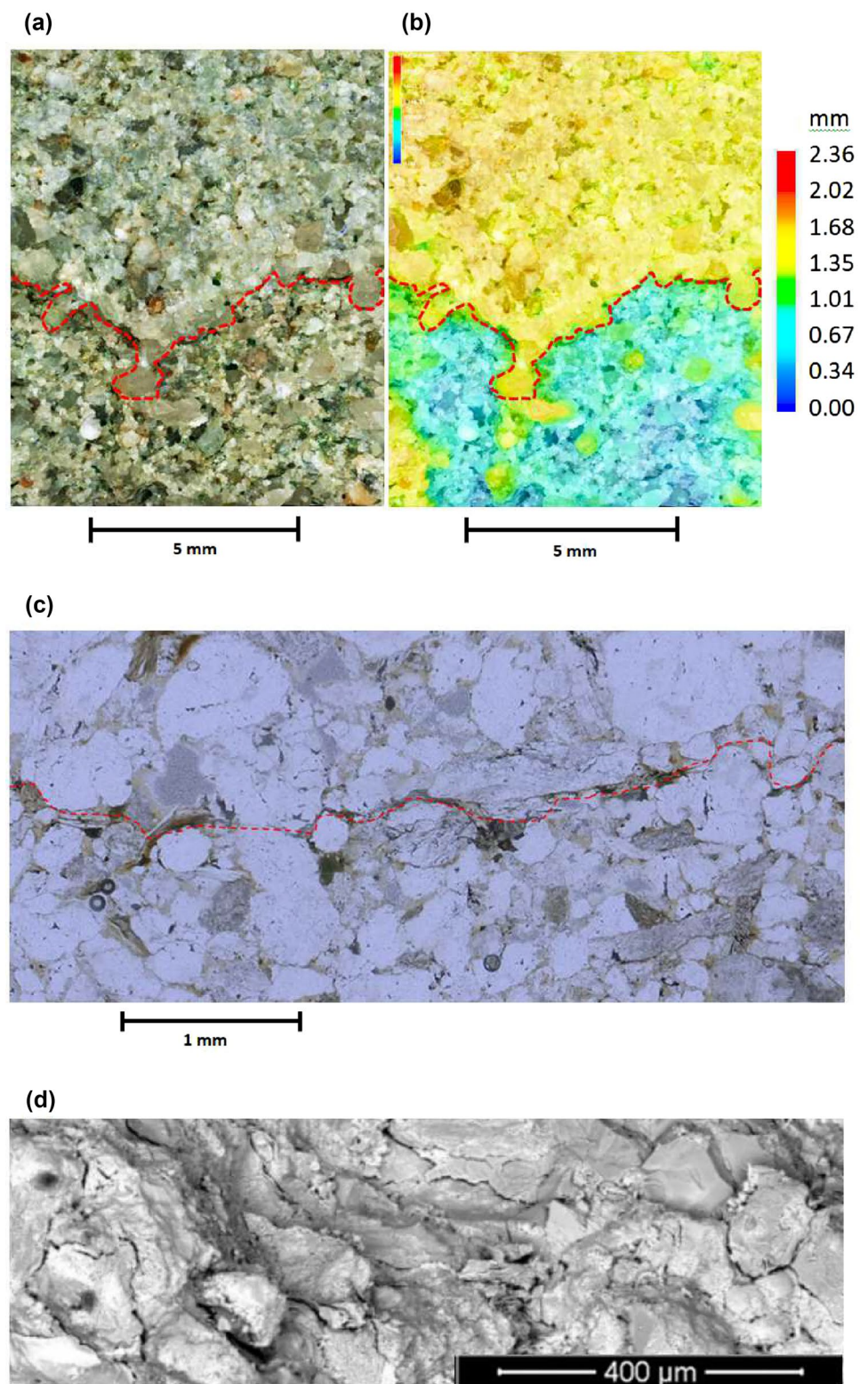
corresponded to the area in the images **a**, **b** (dark/bright area means lower/higher X-ray adsorption); and **d** the same CT scan in the contrast pseudo-colors for a better comparison with the structures in the image **b** (the dark blue regions have a low absorption of X-rays) (Colors online)

3.2 Model Examples of the Effect of Idealized Material Inhomogeneities in the Form of Layers on Effective Stiffness Moduli

The main difference in the structure of the real samples analyzed in the previous subsection lies in the different typical orientations of the layers, i.e., rather horizontal or with a declination from the horizontal direction. Therefore, two model samples with qualitatively different orientations of the bi-layers, horizontal and oblique (with a declination angle of about 17°), were considered, as described in Sect. 2.4. In addition, a homogeneous sample without a bi-layer was simulated to test the effect of the FEM mesh on the numerical accuracy of the calculated results and to tune the mesh density. The mesh density used for the presented simulations was gradually refined to minimize the differences between the effective moduli of the homogeneous sample calculated

under no-friction conditions and the exact values of the input mechanical parameters of the model. The FEM meshes generated for the model of the inhomogeneous sample with layers demonstrate pronounced inhomogeneity, which could also affect the numerical precision of the results. Therefore, other comparative calculations for models with the inhomogeneous FEM meshes were performed for the values of the material parameters of the homogeneous sample (i.e., $E_S = E_W = E$, and $\nu_S = \nu_W = \nu$). The resulting Young's moduli and Poisson's ratios for the two stress conditions considered (axial compression in the CTC test and lateral compression in the CTE test), two friction conditions (no friction and fixation), the homogeneous sample, and heterogeneous samples with two orientations of non-central layers (the horizontal and oblique) with three degrees of weak layer stiffness ($E_W = 1$ GPa, 0.5 GPa, and 0.1 GPa) are summarized in the form of column graphs in Fig. 10.

Fig. 9 Interconnection between two different layers of sandstone: **a** Photo-micrograph obtained using a stereo-microscope; **b** the same photo-micrograph with a color map of heights; **c** detailed photo-micrograph of a thin section prepared from the rock material at another location of the same two adjacent macroscopic layers (the interface between layers is highlighted in red); and **d** SEM micrograph with a detail of a natural fracture surface generated at such an interface after a manual hammer hit test (Colors online)



The sufficient numerical accuracy of the results can be verified by the presented results of the calculations for the homogeneous sample without friction at the pressing ends. For these conditions, the Young's moduli and

Poisson's ratios calculated for CTC and CTE loading of the homogeneous sample were very close to the input theoretical value. This applies to the results of the calculation using the mesh, which was generated directly for a homogeneous

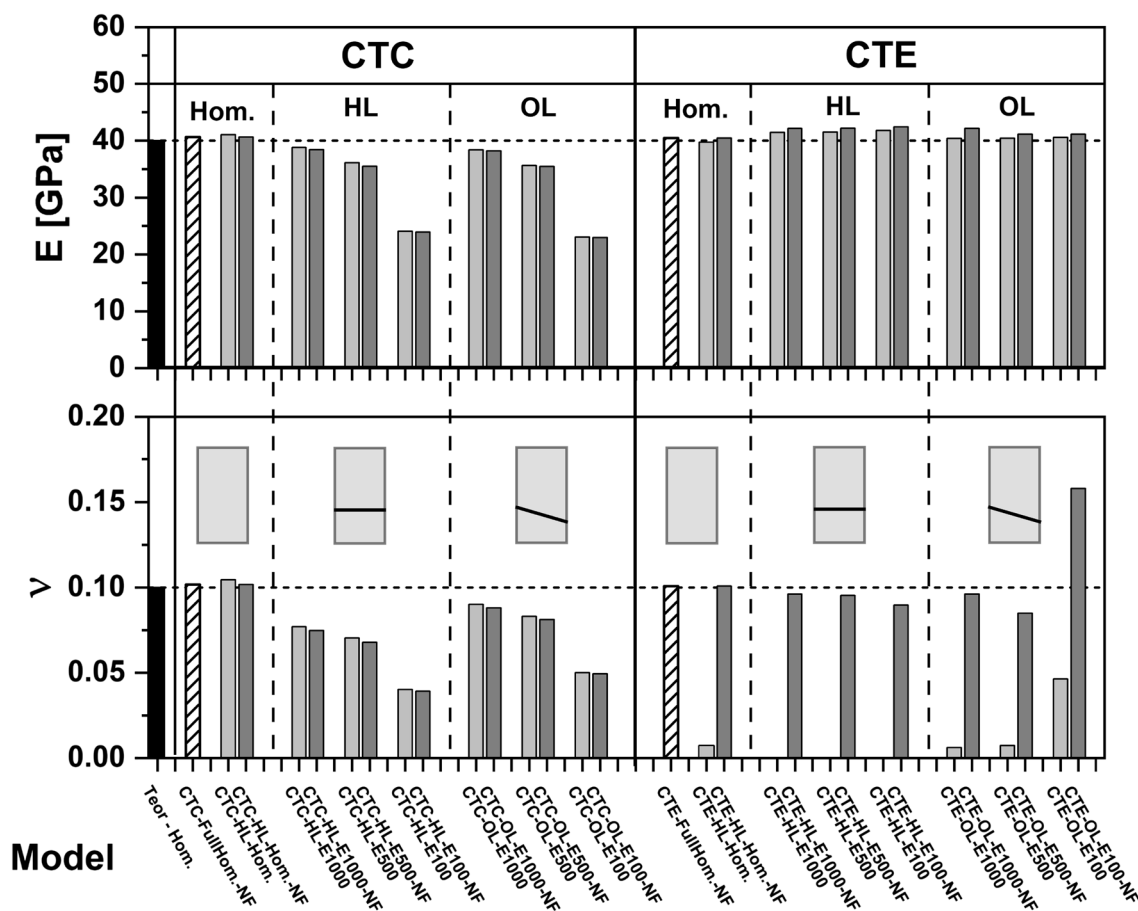


Fig. 10 Results of the idealized FEM model. The resulting Young’s moduli and Poisson’s ratios from the theoretical calculation that simulated the measurement for the CTC and CTE loading applied on a homogeneous sample (Hom.) and two inhomogeneous samples corresponding to two representative orientations of the bi-layer described in the text, i.e., horizontal layer (HL) and oblique layer (OL). Theoretical values for homogeneous (basic) material—a model input (black columns). Hom.: model of a homogeneous sample without any

simulated layers—no friction (NF) at the pressing ends (columns with pattern); model of homogeneous sample with a mesh generated for the model with horizontal layer—fixed ends (light-gray columns) and NF case (dark-gray columns). HL and OL: fixed ends (light-gray columns) and NF case (dark-gray columns); the column labels E1000, E500, E100 correspond to the values of $E_w = 1$ GPa, 0.5 GPa, and 0.1 GPa (see model description in text)

sample, as well as to the results obtained using an inhomogeneous mesh. Even the models with the fixation of the ends yielded results which were almost identical to the values determined for free ends. A notable exception occurred only in the case of the CTE condition, where the value of the Poisson’s ratio was close to zero. However, this anomaly is not a consequence of the inhomogeneity of the FEM mesh. It is the result of a combination of the measurement configuration used and the inhomogeneity of the transverse deformation in the axial direction for the conditions of the fixed ends (compare a similar situation where an axially loaded sample has the well-known “barrel shape”). For these boundary conditions, the same behavior of the determined value of the Poisson’s ratio under CTE loading can be observed for all models of the inhomogeneous sample with layers. However, these extreme

conditions (the assumption of fixed ends) do not correspond to the typical situations, which are rather closer to the approximation of free ends (see, e.g., the experiment in Feng et al. 2017). Therefore, the effect of friction should not be so drastic. In addition, especially under CTE conditions where the axial load is less than for CTC, the friction at the ends should be less. Thus, the following discussion of the results from inhomogeneous sample models will focus only on the friction-free cases. However, the Poisson’s ratio determined for CTE conditions will undoubtedly be very sensitive to changes in the value of friction. In real measurements, the corresponding effective value of the Poisson’s ratio could be somewhat reduced through the existence of nonzero friction at the surfaces of the stiff metallic ends.

Based on the results of models of inhomogeneous samples with layers, the influence of two parameters of the bi-layer

was analyzed: its orientation (horizontal and oblique) and the “weakness” of the thin layer (three degrees of stiffness). Under CTC conditions, the presence of a thin weak layer leads to a decrease in the effective Young’s modulus in the axial direction compared to the E of the dominant material. For the calculated value of this axial modulus, the angle of the layer is not as important as the degree of its stiffness. The same can be drawn for the corresponding Poisson’s ratio, which is also less than the value ν of the dominant material. In the simulated measurement under CTE conditions, the calculated lateral Young’s modulus is slightly higher than the value of E , and the orientation of the layers does not significantly affect its magnitude. On the other hand, for the Poisson’s ratio, this orientation is important, and especially for a very weak oblique layer, the calculated effective Poisson’s ratio can be larger (consequence of shearing). The illustration of the deformation modes under the axial and lateral loads for all discussed sample models can be found in Figs. 11 and 12, respectively.

This FEM model with a linear deformational response, despite its simplicity, provided a basic qualitative estimate of the possible influence of the layered structure of the sample on the measured effective Young’s moduli and Poisson’s ratios. The main trends are the same as for real samples. For horizontally oriented layers, the effective Young’s modulus of a rock sample under CTE conditions is comparable to that determined in the case of layers declined from the horizontal direction. In contrast, the value of the effective Poisson’s ratio is highly sensitive to the orientation of the layer under these conditions. The dispersion of the experimental value of the effective CTE Poisson’s ratio is indeed considerable. The Young’s moduli determined under the CTC loading mode are typically lower than those determined under CTE conditions. The values of the effective Young’s modulus and the Poisson’s ratio from CTC tests are only slightly affected by the orientation of the layers. This fact can explain the typical low variability of the experimental values of these effective CTC moduli measured on samples drilled perpendicular to the macroscopic stratification (i.e., with the expected low local declination of layers from the average direction of stratification). The corresponding axial and lateral strain curves, shown in Fig. 13 for the models with the weakest layer ($E_w = 0.1$ GPa), illustrate the qualitative trends in the behavior of the sample deformation during loading.

The deformation response of the samples in the experiment may not be linear in general due to the gradual damage of the joints in the weakened layers. Therefore, several gradually descending values of the modulus E_w of the weak layer can be considered a model of the gradual weakening of a real thin interlayer (in the sense of continuing damage to local grain joints). This continuous process is the consequence of increasing stress and a wide distribution of the local ultimate strengths of the joints. Such weakening in the

layer material during loading in a direction perpendicular to the layer should generally be less and slower than for shearing and tension loading applied parallel to this layer. Specifically, for the oblique orientation of the layer, this increased weakening under CTE loading may lead to a significant shearing of adjacent surfaces of harder material separated by the thin interlayer. In the case of layers with a significant declination from the horizontal direction, the value of the measured effective Poisson’s ratio can be relatively high.

The results demonstrate that for a given triaxial loading regime, the orientation of weakened thin layers in rock samples can have a significant effect on the deformation behavior. However, when comparing the effective moduli for different triaxial loading regimes (e.g., CTC and CTE), the effect of intermediate principal stress σ_2 can also be considered. It is well known that an increase in mean stress usually leads to an increase in ultimate peak strength (Takemura et al. 2012), although for very high initial pressures, the effect is gradually suppressed. This effect could, thus, cause an additional increase in the effective Young’s modulus when loading via the CTE path (the maximum value of σ_2) compared to its value determined under the conditions of CTC loading (the minimum value of σ_2). On the other hand, the experiments on “weak” sandstones (Ma and Haimson 2016) have shown that an increase in σ_2 has substantially less effect on the peak strength than the increase in the minimal principal stress σ_3 . In addition, while the peak strength monotonically increased with the σ_3 , the dependence of the peak strength on σ_2 represents rather a non-monotonic function with a central maximum and close peak strengths for the limit values of σ_2 ($\sigma_2 = \sigma_3$ and $\sigma_2 = \sigma_1$). Thus, the impact of the additional increase in effective modules may not be felt, or at least may not be crucial.

When stiffness moduli from the triaxial test are reported in published papers, it is usually from the standard CTC test. Besides our experiment (Janeček et al. 2024), the work (Panaghi et al. 2021) mentioned in the introduction deals with the comparison of modules determined using CTC and CTE paths. The Young’s moduli determined from the CTE paths are for a given initial pressure higher than those from CTC paths, which corresponds to the trends observed in our experiments. The behavior of Poisson’s ratios did not exhibit a pronounced trend. The comparison of the published results is complicated by the fact that the work does not state whether the biaxial nature of the additional load was taken into account during their evaluation.

As concluded, latent defects in the form of weakened layers can significantly affect the measured effective stiffness moduli. To perform geotechnical estimations and numerical models, obtaining representative values of the moduli is crucial. In addition to the standard techniques used to select representative samples for mechanical measurements (visual inspection of grain size anomalies and obvious defects, differences in bulk density, anomalous ultrasonic velocity, etc.),

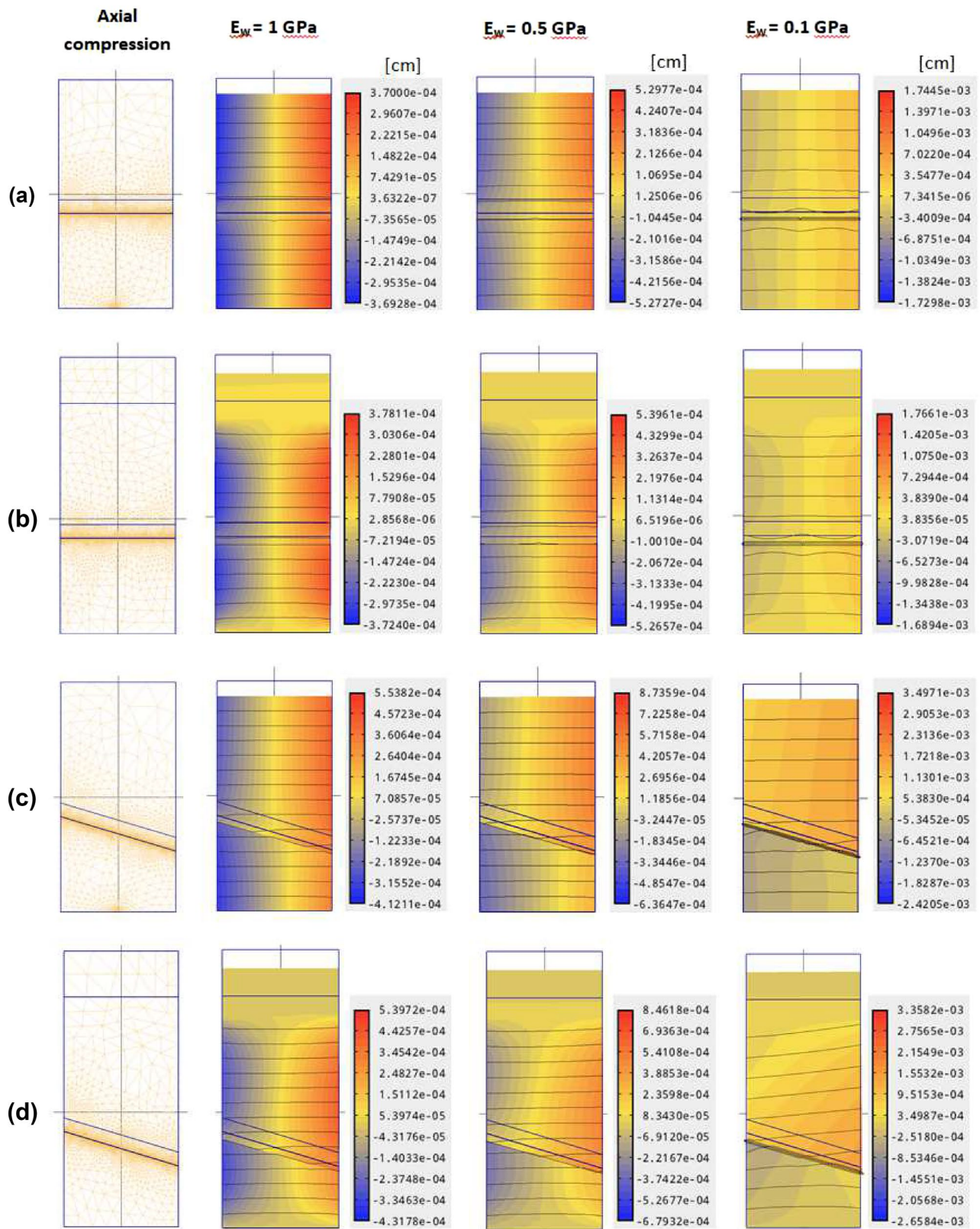


Fig. 11 Deformation modes of samples under axial load in the FEM model. Graphical outputs from Agros2D: shape—rescaled deformation (a.u.); contours—displacement (a.u.); colors—horizontal displacement (scales on the right). Rows: **a, b** sample with horizontal layer (no friction and fixed ends); **c, d** sample with oblique layer (no friction and fixed ends). Images in the first column on the left—FEM mesh (Colors online)

tion and fixed ends); **c, d** sample with oblique layer (no friction and fixed ends). Images in the first column on the left—FEM mesh (Colors online)

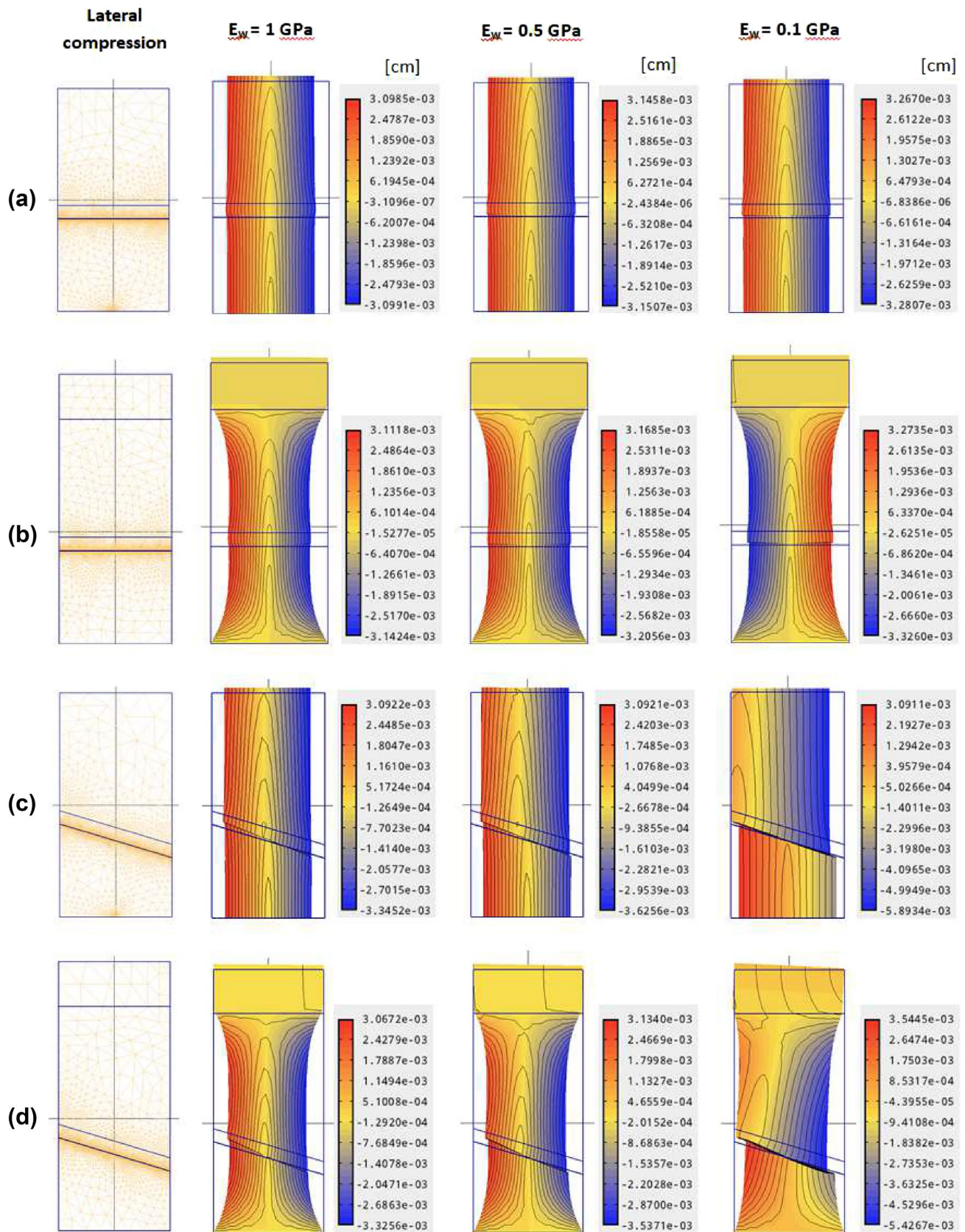


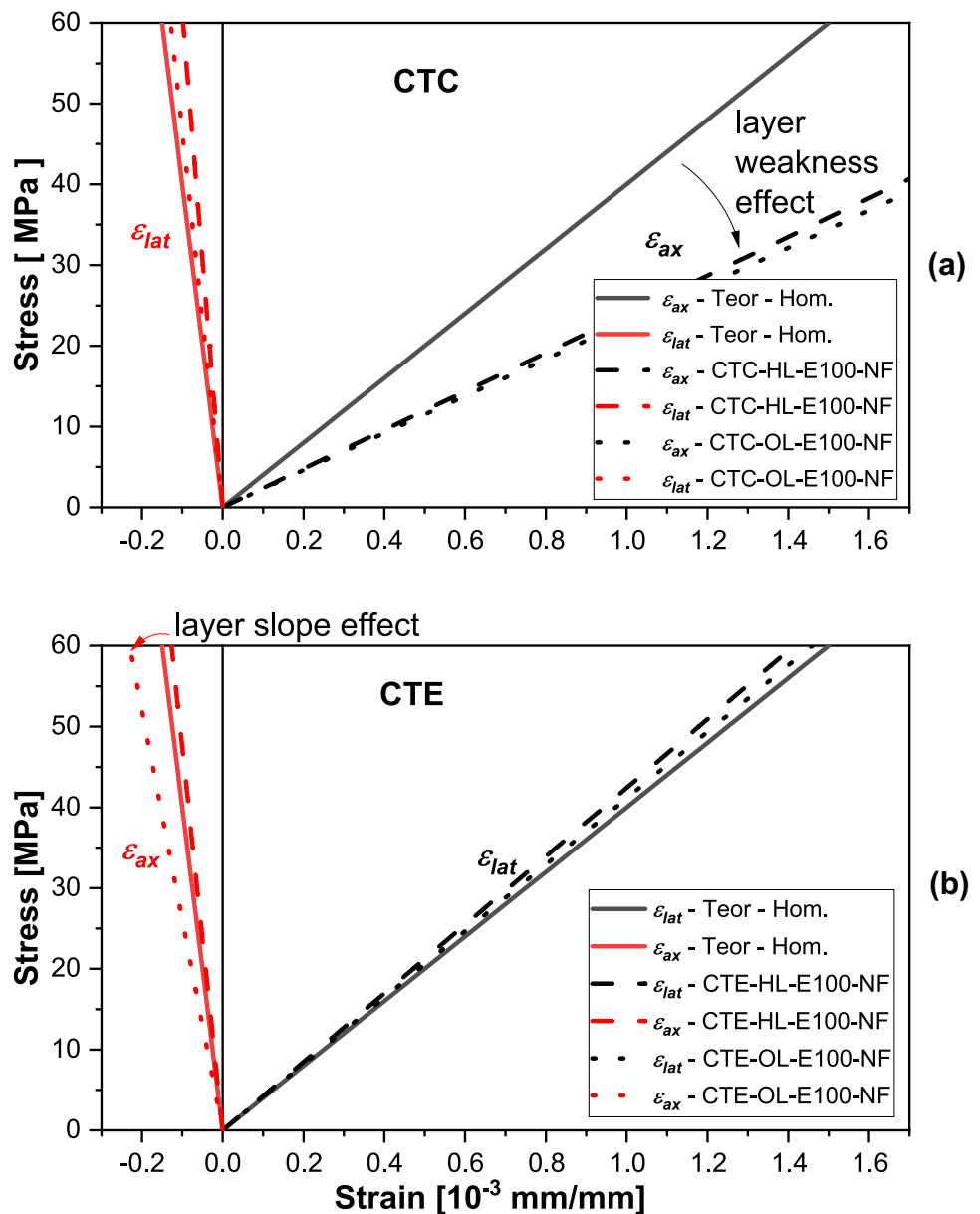
Fig. 12 Deformation modes of samples under lateral load in the FEM model. Graphical outputs from Agros2D: shape—rescaled deformation (a.u.); contours—displacement (a.u.); colors—horizontal displacement (scales on the right). Rows: **a, b** sample with horizontal layer (no friction and fixed ends); **c, d** sample with oblique layer (no friction and fixed ends). Images in the first column on the left—FEM mesh (Colors online)

it is also appropriate to analyze the presence of latent defects in rock using further methods. Besides detailed X-ray CT analyses, a technique using a water jet can be applied.

3.3 Discussion of the Applicability of the Water Jet Erosion Method

Sedimentological studies based on texture analysis sometimes require highlighting the arrangement of the rock material. Moreover, in geotechnical experiments with the deformation of standard rock samples prepared by drilling from blocks taken from a quarry, it is necessary to have a series of samples in the experiment that have a close texture and structure. This is especially relevant for sedimentary clastic rocks that come from layered bodies formed as turbidite sediments, or rocks formed as river sediments. These are usually arkoses, greywackes, and sandstones with vaguely demarcated laminae of siltstones. Alternatively, it can be conglomerates with a supporting framework of

Fig. 13 Illustration of strains from the FEM model. Axial and lateral strains for model samples under loading by **a** axial stress (CTC case) and **b** lateral stress (CTE case): ideal homogeneous sample (Teor-Hom.) and inhomogeneous samples containing a bi-layer ($E_w = 0.1$ GPa) with horizontal (HL) or oblique (OL) orientation. The FEM model without fixation of ends (NF). See the description of the models in the text (Colors online)



sandstones, siltstones, or claystones. In these turbidity sediments, alternation of thin layers of clay, sandstones, or siltstones often is observed. In addition to primary textures, these rocks often also show diagenetic to anchimetamorphic cementation. This is caused, for example, by the deposition of pyrite, carbonates, limonite, glauconite, phosphates, opal, and quartz. The cementation may not be uniform throughout the entire volume of the test specimen and is concentrated, for example, in concretions, laminae, etc. Differences in the cementation cause different resistance to water jet erosion, which predetermines it as a tool for analyzing the heterogeneous rock structure. A description of the textural composition of these rocks only by visual inspection (or other standard techniques) is sometimes difficult. Precisely in these cases, it is appropriate to use erosion by a high-pressure water jet, as demonstrated by the results of this study (Sect. 3.1). Our preliminary internal tests have confirmed that the water jet erosion method can be applied to some other types of sandstones. Pronounced erosion reliefs very well revealed the internal structure in the majority of these rocks. On the other hand, very homogeneous sandstones (or siltstones) show after water jet erosion only uniformly roughened surfaces. The effects of water jet erosion were also tested on other types of rocks. However, typical uniform igneous rocks such as granite do not usually show well-structured relief. In the case of other genetic types of rocks, the same procedure can be used to distinguish the material that can be more easily eroded, i.e., material with less bond strength. These are, e.g., metamorphic rocks with developed foliation (S-tectonites) defined by the mineral composition and structure, and with layer thicknesses ranging from millimeters to centimeters. Good highlighting of the layered structure by the water jet erosion was achieved in the green slate. Another useful application of this technique was, for example, the mapping of the position of garnet grains in gneisses. The reader can find selected examples of erosion relief obtained by applying a water jet to different types of rocks in the supplementary material. In addition to the analysis of the rock structure, this method can be used to investigate the structure and defects of building materials such as concrete.

4 Conclusion

The main focus of this study was the detailed analysis of irregularities in the inhomogeneous layered structure of the selected sedimentary rock (Brenna sandstone), which may be responsible for the different deformational behavior of the compact rock samples under identical triaxial loading modes. The important initial goal was, therefore, to find methods that would well depict the morphology of such structures and provide basic information about their nature or mechanical resistance. Several selected physical techniques,

including a new method using controlled water jet erosion, were applied to visualize the layered structure of the Brenna sandstone from the Beskid Mountains in the Silesian region. The results obtained by all these techniques were compared. In addition, the role of an idealized layered structure in the mechanism of the deformational response of measured samples was analyzed through numerical simulations based on an illustrative simple linearized model. The conclusions and benefits of this study can be summarized as follows:

- A new method combining water jet erosion and 3D visual scanning was applied to analyze the internal structure and mechanical resistance of the rock material in the samples. The combination of these techniques enabled the best visualization of the layered inhomogeneities in the material. This method, thus, offers a promising alternative way for quickly analyzing the structure of rock samples tested in geoengineering projects.
- The benefit of this method is that the material texture and morphology of the layers in sedimentary rocks visualized in the form of the rock surface erosion relief created after a short application of a water jet is usually more obvious than, for example, in the pictures which were obtained by time-consuming X-ray CT scanning. Thus, the water jet erosion method is particularly suitable for contrast visualization of the material texture in the sedimentary rocks. However, it can also be successfully applied to study the morphology of other types of inhomogeneous rocks consisting of materials with different mechanical resistances. The important advantage of the new method is that it displays the texture even in cases where it is difficult to determine it well visually.
- The layers visualized in the Brenna sandstone correspond to materials with different densities and mechanical resistance. Stronger layers represented the places with increased silicification of the grains. The weak interface between these strong and less mechanically resistant layers may be associated with latent fracture surfaces.
- The importance of the identified weakened layers for the mechanical behavior of sandstone lies in the fact that the gradual micro-crushing of weak joints in these layers under load causes their compression or shearing of adjacent regions in the rock. Although these defects of basic rock material are often latent, they can substantially affect the behavior of effective stiffness moduli in the quasi-elastic stress region. The experimentally observed variability of these moduli can be qualitatively explained by the mechanics of defects in the form of thin weak layers with different orientations.
- The idealized numerical model showed that, in addition to the degree of thin layer weakening, its orientation has a crucial influence on the different behavior observed in the identical CTE modes. Despite

the simplicity of this model, the observed trends in deformation under the simulated triaxial conditions qualitatively correspond to the experimental results. For example, the highest variability was observed for Poisson's ratio under simulated conditions corresponding to the CTE test.

- Therefore, such inhomogeneities can visibly affect the measured effective stiffness moduli, especially the Poisson's ratio measured under CTE conditions. Determining a representative effective value of the Poisson's ratio is important, for example, for estimating the stress states of sedimentary basins considered for the construction of geothermal systems.
- This study showed that for more accurate estimates of the mechanical properties of rocks, attention should be devoted to the inhomogeneous evolution of deformation under different modes of loading due to the existence of latent defects in tested samples. Although rock mechanics standards recommend using macroscopically homogeneous samples for measurement of the mechanical characteristics, the initial homogeneity of mechanical cohesive bonds may not be well met even in very compact rocks with uniformly distributed mass density. These effects are usually not taken into account in measurements determining the stiffness moduli for the models in geoenvironmental practice.

Supplementary Information The online version contains supplementary material available at <https://doi.org/10.1007/s00603-024-03828-3>.

Funding Open access publishing supported by the National Technical Library in Prague. This work was supported by the following projects: Grant No. CZ.1.05/2.1.00/03.0082—"Institute of Clean Technologies for Mining and Utilization of Raw Materials for Energy Use" of the "Research and Development for Innovations Operational Programme," co-financed by Structural Funds of the European Union (financial support for the equipment of the rock mechanics laboratory and verification of measurement methodologies); Grant No CZ.02.1.01/0.0/0.0/16_013/0001792—"RINGEN-Research Infrastructure for Geothermal Energy-Upgrade" of "Operational Programme Research, Development and Education" financial support for experiments; Grants Nos. 23-07415S and 23-05128S from the Czech Science Foundation (financial support for the testing of water jet technology and X-ray CT analyses); and Open access publishing supported by the National Technical Library in Prague.

Data Availability Data will be made available on reasonable request.

Declarations

Conflict of interest The authors declare that they have no conflict of interest and no financial and personal relationships with other people or organizations that can inappropriately influence our work. There is no professional or other personal interest that could be construed as influencing the review of this manuscript.

Open Access This article is licensed under a Creative Commons Attribution 4.0 International License, which permits use, sharing,

adaptation, distribution and reproduction in any medium or format, as long as you give appropriate credit to the original author(s) and the source, provide a link to the Creative Commons licence, and indicate if changes were made. The images or other third party material in this article are included in the article's Creative Commons licence, unless indicated otherwise in a credit line to the material. If material is not included in the article's Creative Commons licence and your intended use is not permitted by statutory regulation or exceeds the permitted use, you will need to obtain permission directly from the copyright holder. To view a copy of this licence, visit <http://creativecommons.org/licenses/by/4.0/>.

References

- Arns CH, Knackstedt MA, Pinczewski MV, Lindquist W (2001) Accurate estimation of transport properties from microtomographic images. *Geophys Res Lett* 28:3361–3364
- Baud P, Louis L, David C, Rawling GC, Wong TF (2005) Effects of bedding and foliation on mechanical anisotropy, damage evolution and failure mode. *Geol Soc Lond Spec Publ* 245:223–249
- Crusoe GE Jr, Cai QX, Shu JS, Han L, Barvor Y (2016) Effects of weak layer angle and thickness on the stability of rock slopes. *Int J Min Geoeng* 50:97–110
- Feng XT, Zhang X, Yang C, Kong R, Liu X, Peng S (2017) Evaluation and reduction of the end friction effect in true triaxial tests on hard rocks. *Int J Rock Mech Min Sci* 97:144–148. <https://doi.org/10.1016/j.ijrmm.2017.04.002>
- Gatelier N, Pellet F, Loret B (2002) Mechanical damage of an anisotropic porous rock in cyclic triaxial tests. *Int J Rock Mech Min Sci* 39:335–354
- Hamblin WK (1965) Internal structures of homogeneous sandstones, vol 175. University of Kansas, Topeka
- Hlaváček P, Sitek L, Klichová D, Bodnárová L (2019) Effects of abrasives during accelerated simulation of mechanical corrosion of cement composites using abrasive water flow. *Acta Polytech CTU Proc* 22:31–37
- Honl M, Schwieger K, Carrero V, Rentzsch R, Dierk O, Dries S, Pude F, Bluhm A, Hille E, Louis H et al (2003) The pulsed water jet for selective removal of bone cement during revision arthroplasty. *Biomedizinische Tech Biomed Eng* 48:275–280
- Hu SC, Tan YL, Zhou H, Guo WY, Hu DW, Meng FZ, Liu ZG (2017) Impact of bedding planes on mechanical properties of sandstone. *Rock Mech Rock Eng* 50:2243–2251
- Jamshidi A, Torabi-Kaveh M, Nikudel MR (2021) Effect of anisotropy on the strength and brittleness indices of laminated sandstone. *Iran J Sci Technol Trans A Sci* 45:927–936
- Janeček I, Mishra DA, Vishnu CS, Ščučka J, Vaculíková L, Martinec P (2024) Experimental study of compact sandstone deformation under axisymmetric triaxial loading along specific paths in stress space. *Rock Mech Rock Eng* 57(1):97–113
- Karban P, Mach F, Kůs P, Pánek D, Doležel I (2013) Numerical solution of coupled problems using code Agros2D. *Computing* 95:381–408
- Kwaśniewski M (2012) Mechanical behavior of rocks under true triaxial compression conditions—a review. True triaxial testing of rocks. CRC Press/Balkema, Leiden, pp 99–138
- Kwaśniewski M, Takahashi M (2010) Strain-based failure criteria for rocks: state of the art and recent advances. *Rock Mech Civ Environ Eng* 2010:45–56
- Lai J, Liu B, Li H, Pang X, Liu S, Bao M, Wang G (2021) Bedding parallel fractures in fine-grained sedimentary rocks: recognition,

- formation mechanisms, and prediction using well log. *Petrol Sci* 19:554–569
- Lindquist WB, Venkatarangan A, Dunsmuir J, Wong TF (2000) Pore and throat size distributions measured from synchrotron X-ray tomographic images of Fontainebleau sandstones. *J Geophys Res Solid Earth* 105:21509–21527
- Liu S, Huang Z (2021) Analysis of strength property and pore characteristics of Taihang limestone using X-ray computed tomography at high temperatures. *Sci Rep* 11:1–14
- Louis L, David C, Robion P (2003) Comparison of the anisotropic behaviour of undeformed sandstones under dry and saturated conditions. *Tectonophysics* 370:193–212
- Louis L, Wong TF, Baud P (2007) Imaging strain localization by X-ray radiography and digital image correlation: deformation bands in Rothbach sandstone. *J Struct Geol* 29:129–140
- Louis L, Baud P, Wong TF (2009) Microstructural inhomogeneity and mechanical anisotropy associated with bedding in Rothbach sandstone. *Pure Appl Geophys* 166:1063–1087
- Ma X, Haimson B (2016) Failure characteristics of two porous sandstones subjected to true triaxial stresses. *J Geophys Res Solid Earth* 121:6477–6498
- Momber A (2006) A transition index for rock failure due to liquid impact. *Wear* 260:996–1002
- Nag A, Hloch S, Dixit AR, Pude F (2020) Utilization of ultrasonically forced pulsating water jet decaying for bone cement removal. *Int J Adv Manuf Technol* 110:829–840
- Panaghi K, Takemura T, Asahina D, Takahashi M (2021) Effects of stress path on brittle failure of sandstone: difference in crack growth between tri-axial compression and extension conditions. *Tectonophysics* 810:228865
- Song LT, Liu ZH, Zhou CC, Yu J, Xiu LJ, Sun ZC, Zhang HT (2017) Analysis of elastic anisotropy of tight sandstone and the influential factors. *Appl Geophys* 14:10–20
- Takemura T, Suzuki K, Golshani A, Takahashi M (2012) Stress path dependency of failure mechanism from the viewpoint of dilatant behavior. True triaxial testing of rocks. CRC Press/Balkema, Leiden, pp 203–210
- Vavro M, Vavro L, Martinec P, Souček K (2016) Properties, durability and use of glauconitic Godula sandstones: a relatively less known building stone of the Czech Republic and Poland. *Environ Earth Sci* 75:1–17
- Wei Y, Liu W, Hou Z (2021) Experimental study on the anisotropic characteristics and engineering application of tight sandstone. *Adv Mater Sci Eng* 2021:1–12
- Yiyu L, Fei H, Xiaochuan L, Xiang A (2015) On the failure pattern of sandstone impacted by high-velocity water jet. *Int J Impact Eng* 76:67–74
- Ziccarelli M, Rosone M (2021) Influence of a thin horizontal weak layer on the mechanical behaviour of shallow foundations resting on sand. *Geosciences* 11:392

Publisher's Note Springer Nature remains neutral with regard to jurisdictional claims in published maps and institutional affiliations.